# A single van der pol wake oscillator model for coupled cross-flow and in-line vortex-induced vibrations

Qu, Yang; Metrikine, Andrei V.

**DOI**
10.1016/j.oceaneng.2019.106732

**Publication date**
2020

**Document Version**
Accepted author manuscript

**Published in**
Ocean Engineering

# A single van der Pol wake oscillator model for coupled cross-flow and in-line vortex-induced vibrations

Yang Qu[a,*], Andrei V. Metrikine[a,b]

[a] *Department of Hydraulic Engineering, Delft University of Technology, Stevinweg 1, 2628CN Delft, The Netherlands*
[b] *Department of Engineering Structures, Delft University of Technology, Stevinweg 1, 2628CN Delft, The Netherlands*

## Abstract

In this study a new wake oscillator model is proposed to describe the coupled cross-flow and in-line vortex-induced vibrations of an elastically supported rigid cylinder. Different from many other studies where two wake oscillators have been applied, the current model uses only one wake oscillator coupled to both cross-flow and in-line motions. The new model is based on the van der Pol oscillator with the classic acceleration coupling between the wake and cross-flow motion, while the in-line motion is coupled with the wake variable in a nonlinear manner. The predictions of this new model are compared with the existing experimental data and shown to be in good agreement. In addition to the conventional lock-in range that corresponds to reduced velocities between 5 and 8, another lock-in is predicted around reduced velocity of 2.5 due to the in-line vibration. Most importantly, the new model is proved to be able to predict the appearance of the 'super-upper' branch at small mass ratios without changing the tuning parameters. The limitations of the model associated with unrealistic predictions of free vibrations with very small mass ratios and those of forced in-line vibrations at high frequencies are also discussed along with a possible remedy.

*Keywords:* vortex-induced vibration, coupled cross-flow and in-line vibration, wake oscillator model, fluid-structure interaction

## 1. Introduction

Vortex-induced vibration (VIV) is a well-known phenomenon to civil engineers as it often occurs in flexible cylindrical structures, such as chimneys, cables of suspended bridges, suspended power lines, offshore risers and mooring cables, that are subjected to air or water flows. This vibration can lead to the rapid accumulation of fatigue damage, or it can even result in the sudden collapse of a structure.

Due to the complexity of the fluid-structure interaction problem, most knowledge about VIV to date has been obtained from physical experiments. It is the VIV of rigid cylinders that has been the focus of early research. Two types of experiments have been adopted by the majority of researchers to investigate the problem: free and forced vibration tests. In the free vibration

*Corresponding author
*Email address:* y.qu-1@tudelft.nl (Yang Qu)

tests an elastically supported rigid cylinder vibrates due to the fluid-structure interaction, and the characteristics of the motion are analysed. The forced vibration test, on the other hand, investigates the hydrodynamic forces acting on and the wake structure behind a cylinder that is forced to vibrate with constant amplitude and frequency. Reviews of these studies can be found in the papers by Williamson and Govardhan (2004) and Sarpkaya (2004). The accumulated results from the investigation of the VIV of rigid cylinders have provided some insights into the fundamental mechanism of VIV, and several prediction models have been developed.

So far the prediction of VIV mainly relies on the semi-empirical approaches such as force-decomposition methods, wake oscillator models, single degree-of-freedom models and variation approach. A detailed review of these approaches can be found in the paper by Gabbai and Benaroya (2005). In particular, the wake oscillator model has been the focus of many works in recent years. The fundamental idea of this approach is to describe the dynamics of the wake using an effective nonlinear oscillator, whose motion is coupled to the dynamics of the cylinder. Instead of modelling the actual flow field, this model attempts to reproduce the main features of VIV observed in experiments, and it is thus phenomenological. The concept of the wake oscillator can be dated back to the 1950s when Birkhoff (1953) tried to find expressions for the Strouhal frequency and vortex spacing in the wake through a linear oscillator that describes the motion of the angle between the wake axis and incoming flow. Bishop and Hassan (1964) were the first to suggest the idea of using a van der Pol nonlinear oscillator for the description of the hydrodynamic force. A large number of wake oscillators have been proposed since then in the 1970s and 1980s (Hartlen and Currie, 1970; Skop and Griffin, 1973; Iwan and Blevins, 1974; Landl, 1975). In more recent studies, one main contribution is from Facchinetti et al. (2004) in which a classical van der Pol oscillator is used to model the near wake dynamics, and the effects of several types of linear coupling terms (displacement, velocity and acceleration) modelling the fluid-structure interaction are investigated. Facchinetti et al. (2004) found that the acceleration coupling is most appropriate for the modelling of most of the features of VIV. Facchinetti's model was further improved by properly including the effect of the stall term, dropping the assumption of a small angle of attack (Ogink and Metrikine, 2010).

In most previous studies on the modelling of VIV, the in-line response was normally not of interest, as its amplitude is small compared to the cross-flow response. However, due to its doubled oscillating frequency, relative to the cross-flow, the in-line vibration may introduce significant fatigue damage to the structure. Also, studies have demonstrated that the presence of the in-line vibration may alter the wake pattern and consequently influence the cross-flow response (Dahl et al., 2007; Jauvtis and Williamson, 2004). More importantly, in practical situations, the flexible structures possess multiple natural frequencies and are usually allowed to vibrate in different directions. In such cases, it is possible that resonance occurs in both cross-flow and in-line directions. Therefore, an advanced model that is capable of predicting the coupled cross-flow and in-line VIV is necessary to simulate practically relevant situations.

Although a large number of wake oscillator models have been developed for the prediction of the cross-flow response of a structure, only a few attempts have been made to model the coupled cross-flow and in-line VIV (Kim and Perkins, 2002; Srinil and Zanganeh, 2012; Bai and Qin, 2014; Postnikov et al., 2017). For the latter, the approach of introducing a second nonlinear wake oscillator for the description of the oscillating drag force, in addition to the wake oscillator that describes the lift force, has been widely employed; see, for example, Srinil and Zanganeh (2012); Postnikov et al. (2017); Kim and Perkins (2002). Efforts have been made to tune the model to the experimental measurements, and the influence of the empirical parameters on the simulation results has been investigated (Srinil and Zanganeh, 2012; Postnikov et al., 2017).

Although good agreements between the simulation and experiments have been achieved, the phenomenon of the super-upper branch – characterised by the appearance of a large amplitude of cross-flow vibration at a small mass ratio (Jauvtis and Williamson, 2004) – which is one of the most important characteristics of coupled cross-flow and in-line VIV, has not yet been captured. The simulations and experiments are matched by applying different tuning parameters each time the experimental conditions, such as mass ratio for example, change (Srinil and Zanganeh, 2012). Also, in most literature, only the amplitude of the vibration of the structure is presented, whether these models are able to capture the frequency lock-in around reduced velocity 2.5, which is another main characteristic of the coupled cross-flow and in-line VIV, is not reported.

Introducing a second wake oscillator equation that is coupled with the in-line motion to describe the oscillating drag force is a common approach taken by most researchers. However, in most cases, such as the models by Srinil and Zanganeh (2012); Postnikov et al. (2017), the two wake oscillators are uncoupled (here the uncoupling means that the two oscillators are not directly coupled, in the case of free vibration they are indirectly coupled through the instantaneous flow), and the one that describes the lift force is solely dependent on the cross-flow motion of the cylinder, while the oscillating drag force is predicted by the other oscillator, which is only coupled with the in-line motion. This is not entirely consistent with the fact that the lift and drag forces have the same origin, the dynamics of the wake, and are interdependent on each other. This interdependency is reflected by the fact that there is a certain phase relation between the fluctuating lift and drag forces on a fixed cylinder. However, according to the uncoupled double wake oscillator models, the phase relation between the fluctuating lift and drag forces on a stationary cylinder is arbitrary and dependent on the initial conditions of wake variables. The only model that contains coupled double wake oscillators is given by Kim and Perkins (2002). In this model, a set of quadratic couplings between the two wake oscillators have been introduced and qualitatively analysed. However, the large number of tuning parameters makes this model inefficient and less attractive.

The model with two wake oscillators may be said to contradict the fundamental mechanism of coupled cross-flow and in-line VIV. It is physically more reasonable to use only one oscillator to describe the dynamics of the wake, and this oscillator should be coupled to both cross-flow and in-line motions of the cylinder (not the same as the model by Bai and Qin (2014) where the wake oscillator is only coupled with the cross-flow motion). The development of such a wake oscillator model is the main objective of this paper.

In Section 2, the model that describes the two degrees of freedom VIV of an elastically supported rigid cylinder is presented, with the focus on the introduction of an in-line coupling term to the wake oscillator equation. The proposed model is then compared with the free vibration experiments in Section 3. The limitation of the new model under in-line forced vibrations at high frequencies is discussed in Section 4 and a modification of the in-line coupling term is proposed. The modified model is then compared with the original one with respect to the prediction of free vibration experiments in Section 5. Final conclusions are provided in Section 6.

## 2. Model Description

In this section, the governing equations for the motion of an elastically supported rigid cylinder that is allowed to move in both cross-flow and in-line directions, the definition of hydrodynamic forces as well as the wake oscillator that is coupled to both in-line and cross-flow motion are presented.

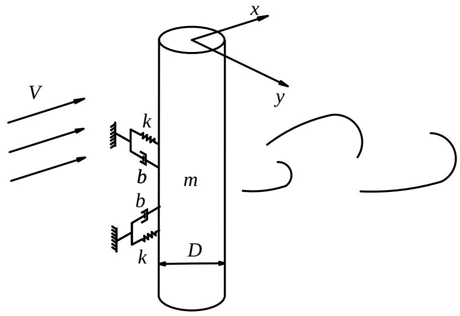


Figure 1: Coupled cross-flow and in-line VIV of an elastically supported rigid cylinder subjects to uniform flow.

### 2.1. Governing equations for the structure

Consider a rigid cylinder that is elastically supported in both cross-flow (represented by the y axis) and in-line (represented by the x axis) directions; see Fig.1. The displacements of the cylinder $X$ and $Y$ along the in-line and cross-flow directions can be described as

$$m\frac{d^2X}{dt^2} + b\frac{dX}{dt} + kX = F_X, \tag{1}$$

$$m\frac{d^2Y}{dt^2} + b\frac{dY}{dt} + kY = F_Y, \tag{2}$$

where $m$ is the mass of the cylinder, and $b$ and $k$ are the viscous damping coefficient and the stiffness of the supports of the cylinder respectively. It should be noted here that there are experiments that have been conducted with unequal mass, stiffness and damping in different directions due to the set-up of the apparatus (Wu and Moe, 1990; Dahl et al., 2006); they are not considered here. Furthermore, $F_X$ and $F_Y$ on the right-hand side of the equations are the in-line and cross-flow hydrodynamic forces acting on the cylinder, both of which are assumed to be expressible as a superposition of a vortex force and an ideal inviscid inertia force associated with the potential added mass of the fluid:

$$F_X = F_{VX} + F_{AX} = \frac{1}{2}\rho D L V^2 C_{VX} - m_a\frac{d^2X}{dt^2} \tag{3}$$

$$F_Y = F_{VY} + F_{AY} = \frac{1}{2}\rho D L V^2 C_{VY} - m_a\frac{d^2Y}{dt^2} \tag{4}$$

In Eqs.(3) and (4), $\rho$ is the mass density of the fluid, $D$ is the diameter, $L$ is the length of the cylinder, $V$ is the undisturbed flow velocity, $C_{VX}$ and $C_{VY}$ are in-line and cross-flow vortex force coefficients respectively, $m_a = C_a\pi\rho D^2 L/4$ is the added mass and the value for $C_a$ is 1, as follows from the potential theory. Moving the potential inertia force to the left-hand side of the equation and dividing the result by $(m + m_a)$, Eqs. (1) and (2) become

$$\frac{d^2X}{dt^2} + 2\zeta\omega_n\frac{dX}{dt} + \omega_n^2 X = \frac{F_{VX}}{m + m_a}. \tag{5}$$

$$\frac{d^2Y}{dt^2} + 2\zeta\omega_n\frac{dY}{dt} + \omega_n^2 Y = \frac{F_{VY}}{m + m_a}. \tag{6}$$

where $\omega_n = \sqrt{k/(m + m_a)}$ and $\zeta = b/(2\omega_n(m + m_a))$ are the natural frequency and damping ratio of the cylinder in still water.

### 2.2. *Definition of hydrodynamic forces*

For an oscillating cylinder, the components $F_{VX}$ and $F_{VY}$ of the vortex force are time-varying hydrodynamic forces which are constructed as the summation of a stall force and a fluctuating excitation component. The concept of the stall force was first suggested by Triantafyllou et al. (1994) according to their experimental finding of a negative slope in the fluctuating lift force and later adopted by Skop and Balasubramanian (1997) and Facchinetti et al. (2004) in their wake oscillator model. It was recently pointed out by Ogink and Metrikine (2010) that the stall term used by Skop and Balasubramanian (1997) and Facchinetti et al. (2004) is the linearised form of instantaneous drag force in the cross-flow direction with the assumption of small angle of attack of the relative flow to the cylinder. It was further suggested by Ogink and Metrikine (2010) that the original nonlinear instantaneous drag force should be used as it gives better match with experiments and also produces fluctuating force in the in-line direction. Therefore, the nonlinear instantaneous drag force model is used in this paper to take into account the stall effect. The instantaneous drag force $F_{VD}$ acts along the relative flow velocity $U$ and can be written as

$$F_{VD} = \frac{1}{2}C_{VD}\rho DLU^2, \tag{7}$$

in which $C_{VD}$ is the drag force coefficient and $U = \sqrt{\left(V - \frac{dX}{dt}\right)^2 + \left(\frac{dY}{dt}\right)^2}$ is the relative flow velocity. Similarly, the instantaneous lift force that is perpendicular to the relatively flow velocity $U$ is given as

$$F_{VL} = \frac{1}{2}C_{VL}\rho DLU^2, \tag{8}$$

where $C_{VL}$ is the instantaneous lift force coefficient which is associated to the wake oscillator. With instantaneous lift and drag forces defined above, the components $F_{VX}$ and $F_{VY}$ of the vortex force then can be written as

$$F_{VX} = \frac{1}{2}C_{VL}\rho DLU^2\sin(\beta) + \frac{1}{2}C_{VD}\rho DLU^2\cos(\beta), \tag{9}$$

$$F_{VY} = \frac{1}{2}C_{VL}\rho DLU^2\cos(\beta) + \frac{1}{2}C_{VD}\rho DLU^2\sin(\beta), \tag{10}$$

in which the angle $\beta$ is the angle between the direction of relative flow velocity $U$ and that of undisturbed flow velocity $V$ and is given as

$$\sin\beta = -\frac{dY}{dt}/U, \text{and} \cos\beta = \left(V - \frac{dX}{dt}\right)/U. \tag{11}$$

The definition of the angle $\beta$ and the force decomposition described above is illustrated in Fig.2.

The force definition described above is the same as the one proposed by Ogink and Metrikine (2010). In their model, the drag force coefficient is assumed to be constant and equals the steady

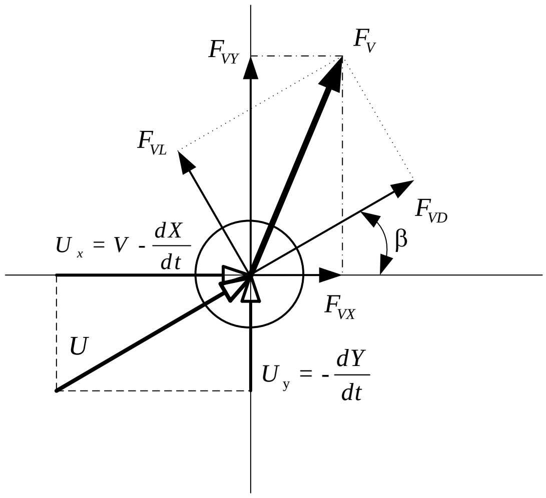


Figure 2: Decomposition of the vortex force in drag, lift, cross-flow and in-line directions (Ogink and Metrikine, 2010).

component of the drag force measured from a stationary cylinder. One main problem with the utilisation of the constant drag force coefficient is that the model is not able to predict pure in-line free vibrations, since the cylinder, according to the force definition, is only subjected to a constant drag force when its motion in the cross-flow direction is constrained. One straightforward approach to deal with this shortcoming is to introduce an oscillating instantaneous drag force that is coupled with the instantaneous lift force in the following form:

$$C_{VD} = C_{DM} + \alpha C_{VL}^2. \tag{12}$$

where $C_{DM}$ is constant, and the second quadratic term describes the relationship between the fluctuating lift and drag forces that are derived from a fixed cylinder (Qin, 2004). According to the definition of Eq.(12), the total drag force is composed of a steady part and an oscillating component. The steady component of the drag force is the summation of $C_{DM}$ and the mean value of $\alpha C_L^2$, and the latter component is proportional to the square of the lift force coefficient's amplitude. Since the steady part of the drag force only damps the energy out from the structure, the author found that the cross-flow motion would be significantly underestimated due to the extra damping introduced by a large lift force. Therefore, in this paper, the instantaneous drag force coefficient is still assumed to be constant $C_{VD} = C_{DM}$. Meanwhile, a fluctuating force is directly introduced in the in-line direction and coupled with the lift force in the same manner as in Eq.(12). In this way, the in-line component $F_{VX}$ of vortex force is reformulated as

$$F_{VX} = \frac{1}{2}C_{VL}\rho DLU^2 \sin(\beta) + \frac{1}{2}C_{DM}\rho DLU^2 \cos(\beta) + \frac{1}{2}\alpha C_{VL}^2 \rho DU_x|U_x|, \tag{13}$$

where $U_x = V - \frac{dX}{dt}$ is the in-line component of the relative flow velocity $U$. When the cylinder dose not move, i.e. $\frac{dY}{dt} = 0$ and $\frac{dX}{dt} = 0$, Eq. (13) reduces to

$$F_{VX} = \frac{1}{2}\left(C_{DM} + \alpha C_{VL}^2\right)\rho DLV^2, \tag{14}$$

which is in the same form as proposed by Qin (2004) for the coupled lift and drag force on a fixed cylinder.

After performing the necessary substitutions into Eqs.(5) and (6), the final equations of motion of the structure can be written as

$$\frac{d^2X}{dt^2} + 2\zeta\omega_n\frac{dX}{dt} + \omega_n^2 X = \frac{1}{2}\rho DV^2\frac{C_{VX}}{m+m_a}. \tag{15}$$

$$\frac{d^2Y}{dt^2} + 2\zeta\omega_n\frac{dY}{dt} + \omega_n^2 Y = \frac{1}{2}\rho DV^2\frac{C_{VY}}{m+m_a}. \tag{16}$$

where

$$C_{VX} = -C_{VL}\frac{U}{V^2}\frac{dY}{dt} + C_{DM}\frac{U}{V^2}\left(V - \frac{dX}{dt}\right) + \alpha C_{VL}^2\left(1 - \frac{1}{V}\frac{dX}{dt}\right)|1 - \frac{1}{V}\frac{dX}{dt}|, \tag{17}$$

and

$$C_{VY} = C_{VL}\frac{U}{V^2}\left(V - \frac{dX}{dt}\right) - C_{DM}\frac{U}{V^2}\frac{dY}{dt}. \tag{18}$$

### *2.3. Wake oscillator coupled to both cross-flow and in-line degrees of freedom of the structure*

When the cylinder is only allowed to move in the cross-flow direction, the dynamics of the wake, which is characterized by alternate vortex shedding, can be described by the van der Pol oscillator forced by structural acceleration as

$$\frac{d^2q}{dt^2} + \epsilon\omega_s(q^2-1)\frac{dq}{dt} + \omega_s^2 q = \frac{A}{D}\frac{d^2Y}{dt^2}, \tag{19}$$

where $q$ is the wake variable and $\omega_s$ is the Strouhal frequency, $\omega_s = 2\pi \mathrm{St}V/D$ in which St denotes the Strouhal number. The parameters $A$ and $\epsilon$ are tuning parameters. The wake variable is related to the lift force coefficient as $C_{VL} = \frac{1}{2}qC_{L0}$ and the reference lift force coefficient $C_{L0}$ is the one measured on a fixed cylinder. It has been proven by Facchinetti et al. (2004) that Eq.(19) is able to model most of the important features of the cross-flow VIV, including the lock-in as a result of wake synchronization driven by the cross-flow motion. In the cross-flow VIV, the use of the oscillator to describe the wake dynamics comes from the experimental observation that 'the wake swings from side to side, somewhat like the tail of a swimming fish' (Birkhoff, 1953) as well as experimental measurements of lift and drag forces that 'responded to forcing rather as a simple oscillator would under similar circumstances' (Bishop and Hassan, 1964). The dynamics of the wake in the cross-flow VIV is dominated by alternating vortex shedding; therefore, the resultant lift force can be reasonably well represented by an oscillator driven by the acceleration of cross-flow motion. Different from cross-flow VIV, for which the dynamics of the wake is dominated by the alternating vortex shedding, the in-line VIV is characterised by two response branches that correspond to different wake patterns. For the first branch (denoted as the SS branch) that occurs at a lower reduced velocity – defined as $V_n = \frac{2\pi V}{\omega_n D}$, within the range roughly between 1 and 2.5 – symmetric vortex shedding is observed, while for the second branch (denoted as the AS branch), the vortices are shed alternatively above $V_n \approx 2.5$, (Aguirre Romano, 1978). The priority of this work is to model the second excitation region of in-line VIV, as it corresponds to wake dynamics that is similar to that in the cross-flow vibration. To simulate the first response branch due to the symmetric vortex shedding, another model may be needed, which is not in the scope of this paper.

In the second excitation region, Konstantinidis (2014) pointed out that the response of the cylinder is steady, and the fluctuation of the wake, represented by the transverse velocity fluctuation, is synchronised to half of the frequency of cylinder oscillation. From forced in-line vibration experiments, Aronsen (2007) also demonstrated that the lift force in this region contains significant components at both 0.5 and 1.5 times the frequency of cylinder oscillation. These facts suggest that the coupling between the in-line motion and the wake variable may be in the form that ensures parametric excitation of the lift force by the in-line vibration. To pursue this idea, the wake oscillator equation is now extended to include a parametric excitation term, and it is given as

$$\frac{d^2q}{dt^2} + \epsilon\omega_s(q^2-1)\frac{dq}{dt} + \omega_s^2 q - \frac{\kappa}{D}\frac{d^2X}{dt^2}q = \frac{A}{D}\frac{d^2Y}{dt^2}. \tag{20}$$

The reason for using $\frac{d^2X}{dt^2}q$ instead of other combinations, such as $\frac{dX}{dt}q$ for example, is a reasonable guess based on the work by Nishi et al. (2008) in which the classic van der Pol wake oscillator equation was derived by replacing the wake behind the cylinder by a rigid bar. The coupling between the dynamics of the rigid bar, represented by the rotation angle, and the cross-flow motion of the cylinder was assumed to follow the same form as the dynamics of a pendulum with a moving suspension point. If the same assumption holds in the in-line direction, then the coupling between the wake oscillator and the in-line motion should be in the form of $\frac{d^2X}{dt^2}q$, as can be derived using the Lagrangian formulism. For a more detailed derivation, please refer to Appendix A.

The wake oscillator, Eq.(20), as well as the structural governing equations Eq. (15) and (16) formulate the initial value problem for the coupled cross-flow and in-line vortex induced vibration of a rigid cylinder. Using the following quantities:

$$\tau = \omega_s t, \Omega_n = \omega_n/\omega_s, x = X/D, y = Y/D, \tag{21}$$

the dimensionless form of the governing equations is obtained as

$$\ddot{x} + 2\zeta\Omega_n\dot{x} + \Omega_n^2 x = \frac{C_{VX}}{2\pi^3\mathrm{St}^2\,(m^* + C_a)}, \tag{22}$$

$$\ddot{y} + 2\zeta\Omega_n\dot{y} + \Omega_n^2 y = \frac{C_{VY}}{2\pi^3\mathrm{St}^2\,(m^* + C_a)}, \tag{23}$$

$$\ddot{q} + \epsilon(q^2-1)\dot{q} + q - \kappa\ddot{x}q = A\ddot{y} \tag{24}$$

where

$$C_{VX} = (C_{DM}\,(1-2\pi\mathrm{St}\dot{x}) + C_{VL}2\pi\mathrm{St}\dot{y})\,\sqrt{(1-2\pi St\dot{x})^2 + (2\pi\mathrm{St}\dot{y})^2} + \alpha C_{VL}^2\,(1-2\pi\mathrm{St}\dot{x})\,|1-2\pi\mathrm{St}\dot{x}|, \tag{25}$$

$$C_{VY} = (-C_{DM}2\pi\mathrm{St}\dot{y} + C_{VL}\,(1-2\pi\mathrm{St}\dot{x}))\,\sqrt{(1-2\pi\mathrm{St}\dot{x})^2 + (2\pi\mathrm{St}\dot{y})^2}. \tag{26}$$

and $C_{VL} = \frac{1}{2}qC_{L0}$, $C_{DM} = C_{D0} - \frac{1}{2}\alpha C_{L0}^2$. Here, $C_{L0}$ and $C_{D0}$ are lift and mean drag force coefficients measured on a fixed cylinder and overdots represent derivative respect to the dimensionless time $\tau$.

## 3. Model predictions of coupled cross-flow and in-line vortex-induced vibrations

With the coupled system defined by Eqs.(22-24), the series of 2DOF VIV experiments reported by Jauvtis and Williamson (2004) have been simulated. In these experiments, the cylinder has the same natural frequency and mass ratio in the cross-flow and in-line directions.

### *3.1. Model predictions of experiments with $m^* = 2.6$ and 7*

Although several experiments have been conducted with mass ratio $m^*$ varying from 1.5 to 25.0 and $(m^* + C_a)\,\zeta$ from 0.001 to 0.1, detailed experimental data of cylinder responses are only reported for the cases of $m^* = 7.0$ with $\zeta = 0.0015$ and $m^* = 2.6$ with $\zeta = 0.0036$. These two cases demonstrate one of the main characteristics of the coupled cross-flow and in-line VIV, namely the phenomenon of the super-upper branch. Jauvtis and Williamson (2004) discovered that the influence of the in-line freedom on the cross-flow response is surprisingly small provided that the mass ratio is higher than $m^* = 6$. However, as the mass ratio becomes smaller than $m^* = 6$, a new response branch, termed a 'super-upper' branch, appears in the cross-flow direction, with a peak cross-flow amplitude as large as $1.5D$. It will be shown later that with the model presented in the current study, this phenomenon is well captured.

The model is first tuned to the measurements with $m^* = 7$. The hydrodynamic coefficients on a stationary cylinder are assumed to be St = 0.2, $C_{L0} = 0.3$ and $\alpha = 2.2$ (to generate an oscillating drag force coefficient around 0.1). The mean drag force coefficient $C_{D0}$ is assumed to be 1.2, then $C_{DM} = C_{D0} - \alpha C_{L0}^2/2 \approx 1.1$. Since the model is not able to predict both the upper and lower branches of the cylinder response simultaneously (Ogink and Metrikine, 2010), two different sets of tuning parameters have been used to capture those branches separately. The case in which the model is tuned to the upper branch is referred to as 'Case U', and the other case is 'Case L'. For practise applications, a new wake oscillator model should be calibrated against a wide variety of experimental data to determine the most suitable empirical and tuning parameters. This requires a comprehensive optimization procedure and a detailed analysis of available experimental measurements. In this paper, we have only conducted a preliminary calibration of the model against the cross-flow response by trial and error. The tuning parameters are determined such that a good compromise between the cross-flow peak amplitude and the shape of the response branch is achieved. The simulation results of the tuned model in comparison with the experimental measurements are illustrated in Fig.3 against reduced velocity. In this figure, $A_x^*$ and $A_y^*$ are dimensionless in-line and cross-flow amplitudes and $\Omega_y$ is the dimensionless cross-flow frequency. Since the calculated responses of the cylinder in both cross-flow and in-line directions are very steady and periodic, $A_x^*$ and $A_y^*$ are determined by finding the maximum recurrent displacements and $\Omega_y$ is found by determining the highest peak in the Fourier spectrum of selected steady state response. The tuning parameters used for Case U are $A = 8$, $\epsilon = 0.08$ and $\kappa = 5$; for Case L, they are $A = 20$, $\epsilon = 0.8$ and $\kappa = 5$.

The simulation results are generally in good agreement with the experimental measurements, and the main characteristics of the coupled cross-flow and in-line VIV are well reproduced. According to the experiments, apart from the conventional lock-in that occurs in the cross-flow-only vibration, an additional lock-in regime, which occurs at lower reduced velocities around $V_n \approx 2.5$, is observed. The latter regime corresponds to the same wake patterns that are observed in the pure in-line vibration with two response branches, SS and AS; therefore, it is denoted as an in-line vibration mode. Since the cross-flow response of the SS branch is almost zero, and the associated wake dynamics with symmetric vortex shedding are not considered by the current model, the results presented next are only for the AS response branch. As can be seen from Fig.3(c), the current model captures the lock-in regime associated with in-line vibration mode well. Within this lock-in range, the simulated frequency of the cross-flow response locks on to half of the natural frequency, $\Omega_y/\Omega_n = 0.5$, which is consistent with the experimental measurements, while the width of the lock-in is smaller than that observed in experiments. This is because, as discussed previously, in the model proposed in this study, only the AS response branch is considered. It is also shown in Fig.3(c) that for Case L there is a peak that reaches the cross-flow natural frequency, $\Omega_y/\Omega_n = 1$, around $V_n = 1.7$. This is not lock-in but a phenomenon of resonance when the third harmonic component in the fluid force approaches the natural frequency of the structure. It needs to be pointed out that there are two predominant frequency components in the spectrum of cross-flow response at reduced velocity $V_n = 1.7$, one corresponds to the Strouhal frequency and the other is the third harmonic. In this specific case the third harmonic component is dominant as a result of resonance while in other cases the Strouhal frequency dominates.

For the response amplitude, as illustrated in Figs.3(a) and (b), the upper and lower response branches are quantitatively captured by Case U and Case L respectively. Coupled cross-flow and in-line motions that are associated with the AS response branch around $V_n \approx 2.5$ are well captured in the Case U, although the predicted AS response branch occurs at slightly smaller reduced velocities, and its cross-flow amplitude is somehow underestimated. As for the in-line response, the amplitude of the AS response is in good agreement with the experiment. The model predictions of the in-line response corresponding to the upper branch of cross-flow vibration is larger than the experimental measurements, and that corresponding to the lower branch is slightly over-predicted by Case L.

With the same tuning parameters, the model is then used to predict the coupled cross-flow and in-line VIV of the experiment with $m^* = 2.6$ and $(m^* + C_a)\zeta = 0.013$. Fig.4 illustrates the prediction of the model in comparison with the experimental measurements. From Fig.4, it can be seen that the agreement between the prediction and experimental measurements is good. The super-upper branch, with the peak amplitude reaching $1.5D$, which is not observed in the previous case ($m^* = 7$) is captured quantitatively. To authors' knowledge, this characteristic of the coupled cross-flow and in-line VIV of rigid cylinders has never been truly captured by any wake oscillator model in the past. The effect of the mass ratio on the prediction of coupled cross-flow and in-line VIV has been considered by Srinil and Zanganeh (2012) who used different empirical and tuning parameters for high, moderate and low mass ratios. This is apparently an alternative approach for practical purposes when the model itself is not able to provide the correct prediction. In another work, Kurushina et al. (2018) conducted optimizations on the nonlinear damping of the wake oscillator equation and associated parameters in order to identify the most suitable wake oscillator models which are applicable to a wide variety of experimental data. They have only obtained such a model for experiments with small mass ratios and a model that is able to cover the whole range of mass ratio is still missing.

The phase difference between the cross-flow and in-line vibrations and the corresponding trajectory shapes of cylinder motion are plotted in Fig.5 in which the phase angle $\phi_{xy}$ is defined in the same way as given by (Jauvtis and Williamson, 2004). It can be seen from Fig.5(a) that the model with the tuning parameters of Case U correctly predicts the general trend of measurements for reduced velocities smaller than 8. However, for the lower branch, while the experimental data are close to 320° with an increased reduced velocity, the predicted phase by Case L continually increases and finally exceeds 360°. The predicted motion trajectory shapes corresponding to specific reduced velocities are depicted in Fig.5(b) based on the last 40 cycles of steady response. In general, the trajectory shapes are consistent with the experimental findings (Jauvtis

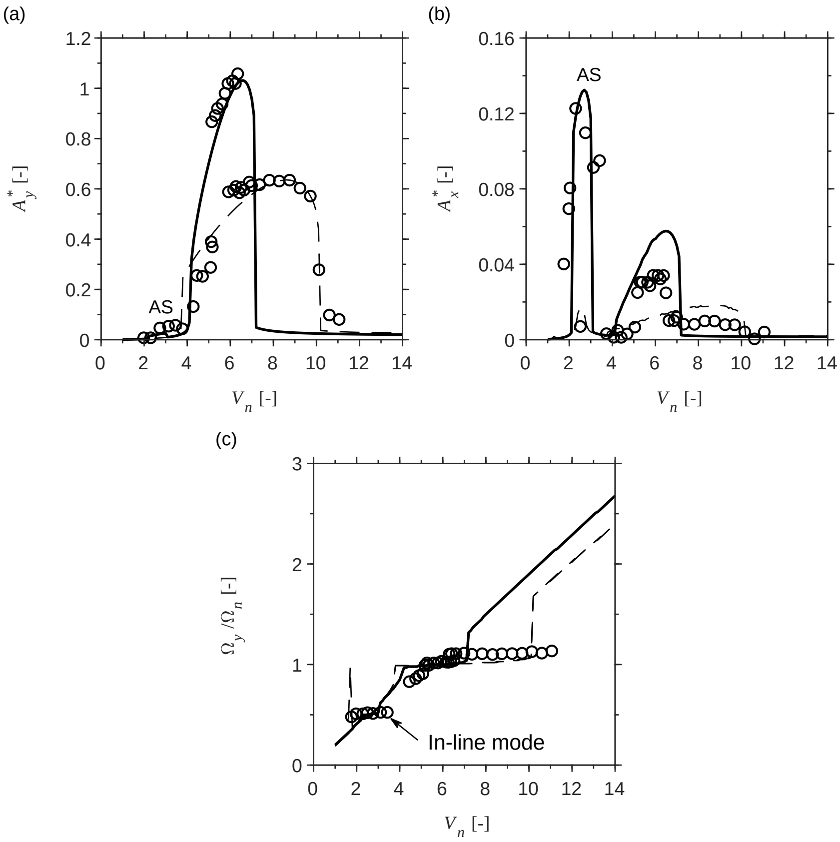


Figure 3: A comparison of numerical (lines) and experimental responses (circles) with $m^* = 7$ and $(m^* + C_a)\,\zeta = 0.0117$ for (a) Cross-flow response amplitude, (b) In-line response amplitude and (c) Normalized cross-flow response frequency. Solid lines represent "Case U", dashed lines represent "Case L", circles represent experimental data

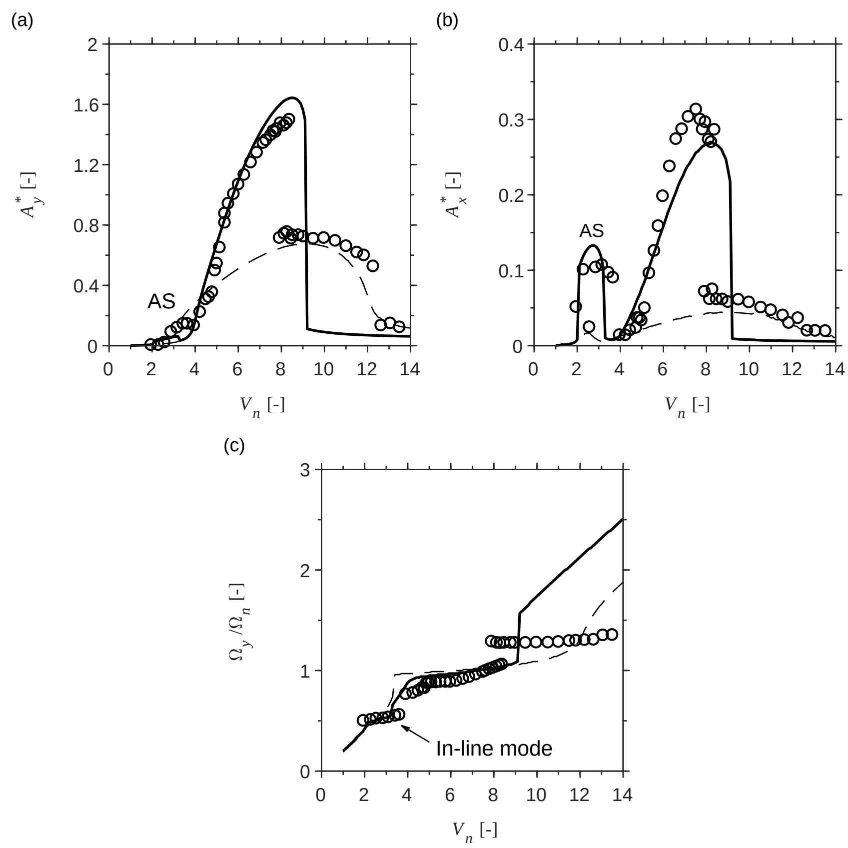


Figure 4: A comparison of numerical (lines) and experimental responses (circles) with $m^* = 2.6$ and $(m^* + C_a)\,\zeta = 0.013$ for (a) Cross-flow response amplitude, (b) In-line response amplitude and (c) Normalized cross-flow response frequency. Solid lines represent "Case U", dashed lines represent "Case L", circles represent experimental data

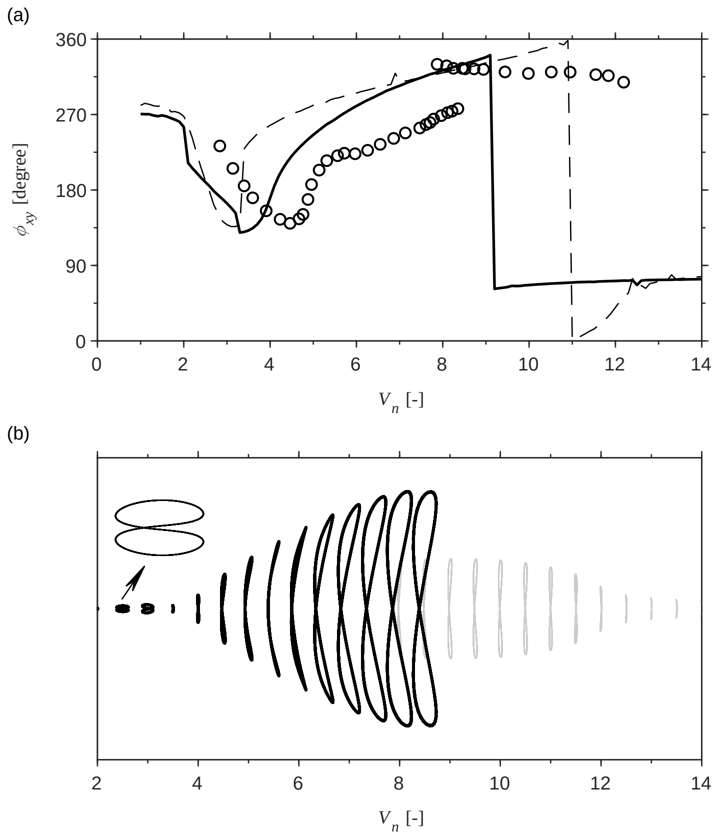


Figure 5: Phase and trajectory of cross-flow and in-line motions with $m^* = 2.6$ and $(m^* + C_a)\,\zeta = 0.013$ for (a) phase angle (solid line represents Case U, dashed line represents Case L, circles represent experimental data) and (b) trajectory (Case U is represented by color black, Case L is represented by color grey).

and Williamson, 2004). For the coupled motion around $V_n \approx 3$, the typical figure-of-eight-type of motion is predicted. As the reduced velocity increases, the figure eight starts to become e-longated in the cross-flow direction and gradually transforms into a crescent pattern. Different from experiments in which the super-upper branch ends with a crescent pattern at the maximum amplitude, the predicted response continues to evolve and ends at the maximum amplitude with a shape of eight again.

### *3.2. Influence of mass ratio and Griffin plot*

In recent decades, discussions have been held as to the main influence factors that affect the maximum amplitude (typically cross-flow) of VIV. Although Govardhan and Williamson (2006) have proven that for the cross-flow-only VIV, it is possible to collapse the peak amplitude data of different cylinders against mass-damping parameter $(m^* + C_a)\,\zeta$ if the influence of the Reynolds number is taken into account, this is most likely not the case for the coupled cross-flow and in-line VIV, as Jauvtis and Williamson (2004) have explicitly demonstrated that the magnitude of the mass ratio plays an important role in the appearance of the super-upper branch that yields large amplitudes in both cross-flow and in-line directions. In this subsection, the proposed model is used to produce the Griffin plots for the coupled cross-flow and in-line VIV and to investigate the influence of the mass ratio on the peak cross-flow and in-line amplitudes. It needs to be pointed out that the Griffin plot shown in this paper is not for the purpose of prediction but to present the model results in a manner similar to how the experimental results were presented. Since the maximum response is focused upon here, only Case U will be considered, and the same tuning parameters as those in Section 3.1 will be used for the rest of this section.

In the series of experiments conducted by Jauvtis and Williamson (2004), although the maximum peak amplitude as function of $(m^* + C_a)\,\zeta$ is reported, in most cases the exact values of $m^*$ and $\zeta$ at which the specific experiment is conducted are not given. Therefore, the simulation results are obtained at several mass ratios picked from the range that is used by the experiments, while the varied $(m^* + C_a)\,\zeta$ is obtained by altering $\zeta$. Fig.6 presents the predicted peak amplitudes of both cross-flow ($A^*_{ymax}$) and in-line ($A^*_{xmax}$) vibrations against $(m^* + C_a)\,\zeta$, with each curve representing a constant $m^*$. It can be seen from Figs.6(a) and (b) that for a specific $(m^* + C_a)\,\zeta$, the predicted peak amplitudes based on different $m^*$ and corresponding $\zeta$ are different, which clearly indicates the effect of $m^*$ in contrast to $(m^* + C_a)\,\zeta$ on the peak amplitude. At a fixed mass ratio, the variation of peak amplitudes against $(m^* + C_a)\,\zeta$ follows the same trend as that observed from cross-flow-only experiments (Govardhan and Williamson, 2006). In general, the peak amplitude first increases rapidly as $(m^* + C_a)\,\zeta$ decreases, and it then gradually reaches a saturation limit when $(m^* + C_a)\,\zeta$ becomes small. The measured cross-flow peak amplitudes are also plotted in Fig.6(a), and it can be seen that these amplitudes for $2.5 < m^* < 4$ (represented by solid dots) are between curves of predictions with $m^* = 3$ and 4.5, which implies that the model predicts slightly higher peak amplitudes at these mass ratios. Those measurements for $6 < m^* < 25$ (represented by circles) are well between curves of predictions with the same mass ratios. With regard to the maximum attainable peak amplitude, the predictions of the model demonstrate the increase in the peak amplitude from around $0.9D$ for a cross-flow response and $0.02D$ for an in-line response at $m^* = 25$ to over $1.9D$ and $0.35D$ respectively at $m^* = 1.5$. It seems that the lower limit of the peak amplitude is reached at $m^* = 25$ for both cross-flow and in-line vibrations, while the upper limits of the cross-flow and in-line peak amplitudes can still be extended as $m^*$ further decreases from 1.5.

To further investigate the influence of $m^*$, the model is used to predict the peak amplitude at a specific $(m^* + C_a)\,\zeta \approx 0.013$ with a varying $m^*$, and the results are presented in Fig.7 in comparison with experimental measurements. Overall, there is a good agreement between the predictions and experimental results over the range of mass ratios reported in the experiments, namely $m^* > 2.5$. The general trend of an increasing peak amplitude with a decreasing $m^*$ is well predicted by the model. For $m^*$ higher than 6, the predicted peak amplitudes in both directions are less dependent on the variation of $m^*$, and they display a trend of convergence as $m^*$ further increases. This is consistent with the experimental observation that at $m^* > 6$, the coupled cross-flow and in-line VIV shows no obvious difference compared to the cross-flow-only VIV, and the peak amplitude, if the influence of the Reynolds number is neglected, mainly depends on the value of $(m^* + C_a)\,\zeta$ ((Govardhan and Williamson, 2006). However, at small mass ratios $m^* < 2.5$, the predicted cross-flow and in-line peak amplitudes keep increasing and reach values over $2.4D$ and $0.45D$ respectively at very small mass ratios, while the experimental data around $m^* = 3$ seem to indicate that both cross-flow and in-line peak amplitudes have a tendency of convergence instead of continuous increase with decreasing mass ratio.

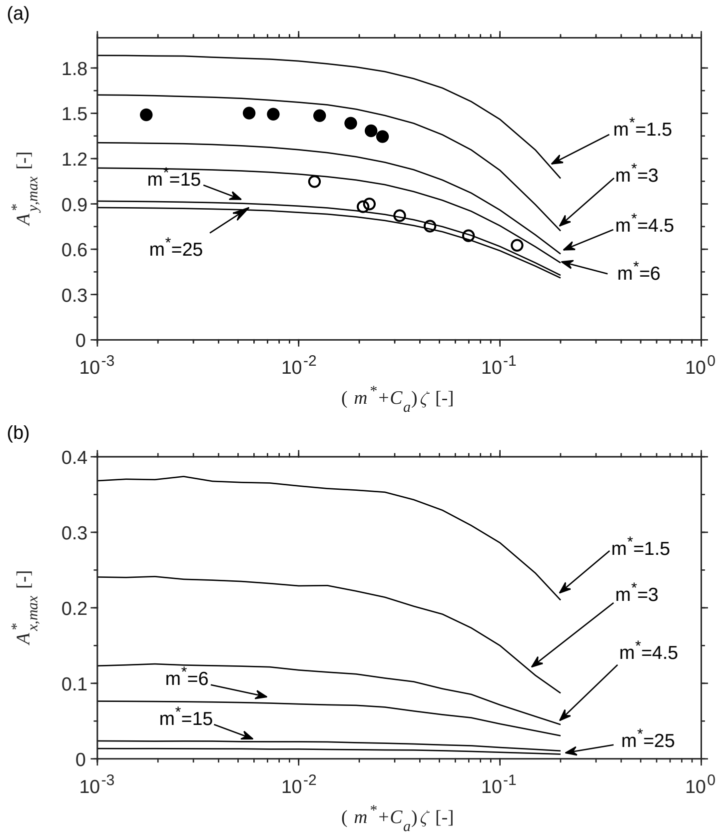


Figure 6: Griffin plots of peak amplitudes for coupled cross-flow and in-line VIV based on experimental (symbols) and prediction (lines) results for (a) Cross-flow peak amplitude and (b) In-line peak amplitude. Dots represent experimental data for $2.5 < m^* < 4$, and circles represent experimental data for $6 < m^* < 25$.

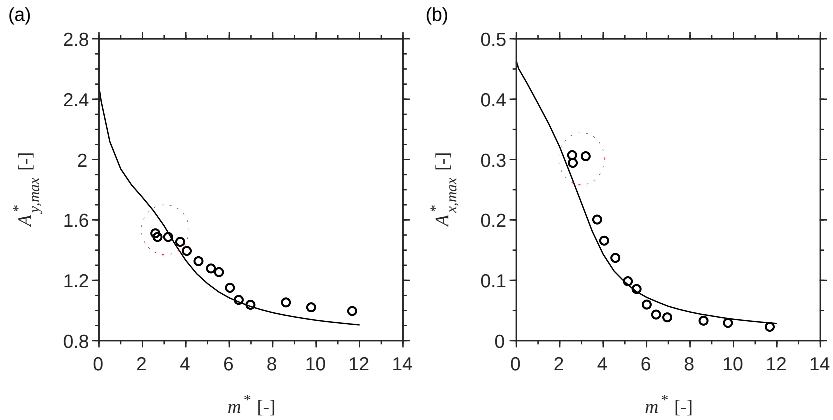


Figure 7: A comparison of predicted (lines) and experimentally measured (circles) peak amplitudes with varying mass ratio for (a) Cross-flow peak amplitude and (b) In-line peak amplitude. The experimental data marked by red circles indicate possible convergence of the peak amplitude with decreasing mass ratio.

## 4. The stability of the new wake oscillator model under in-line forced vibration

Despite of the good performance of the new wake oscillator model in the modelling of coupled cross-flow and in-line free vibrations of an elastically supported rigid cylinder, as shown in previous section, it was discovered by the authors that the model has a stability issue when subjected to forced vibration in the in-line direction. If only the in-line vibration is considered, and ignoring the damping term, then substituting prescribed in-line oscillation $x = x_0 \sin(\Omega\tau)$ into Eq.(24) yields

$$\ddot{q} + q + \kappa\Omega^2 x_0 \sin(\Omega\tau) q = 0. \tag{27}$$

Here, $\Omega$ is given as $\Omega = \omega/\omega_s$, where $\omega$ is the frequency of the prescribed cylinder oscillation. Eq.(27) is of the type generally known as the Mathieu's equation, the stability of which has been studied in detail, and the transition curves that separate stable and unstable regions have been derived (Kovacic et al., 2018). It has been shown that Eq.(27) has several instability zones. The one of most interest to the current study – with $\Omega$ corresponding to reduced velocity $V_r$ smaller than 3, which is associated with the in-line VIV – is plotted in Fig.8(a), with $\kappa = 5$. Here, the definition of the reduced velocity for the forced vibration is given as $V_r = \frac{2\pi V}{\omega D}$. The reduced velocity $V_r$ can also be expressed using dimensionless parameters as $V_r = 1/\mathrm{St}\Omega$.

It can be seen from Fig.8(a) that Eq.(27) is unstable around $\Omega = 2$, and as the amplitude $x_0$ increases, the system is unstable over a wider range of $\Omega$. The instability around $\Omega = 2$, which corresponds to $V_r = 2.5$, is consistent with the experimental observation that in-line VIV occurs around the same reduced velocity and therefore is desirable. However, this unstable region does not have an upper bound with respect to the frequency of oscillation. This instability at high frequencies is against experimental observations, where the synchronisation as well as the amplification of the lift force is bounded within a certain range of frequencies of cylinder oscillation (Nishihara et al., 2005). To enforce the system to be stable at high frequencies of

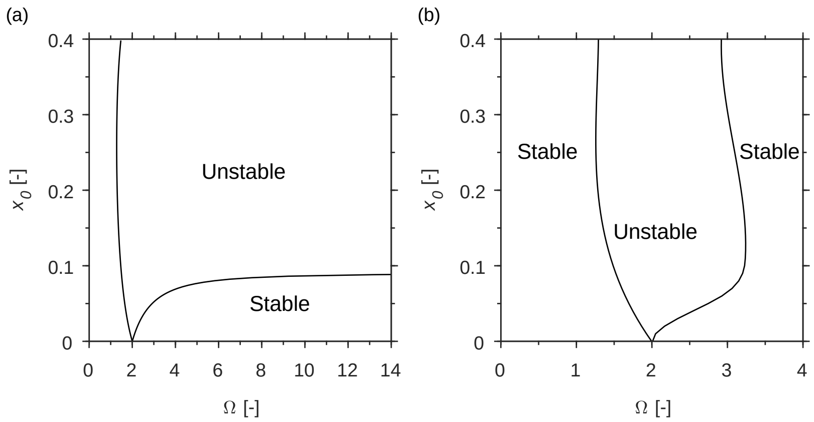


Figure 8: Stability maps of the model with (a) original in-line coupling term and (b) modified in-line coupling term .

in-line vibrations, the term $\ddot{x}q$ is modified into $\frac{\ddot{x}}{1+\ddot{x}^2}q$ so that Eq.(27) becomes

$$\ddot{q} + \epsilon(q^2 - 1)\dot{q} + q - \kappa\frac{\ddot{x}}{1+\ddot{x}^2}q = A\ddot{y}, \tag{28}$$

and the corresponding dimensional form is given as

$$\frac{d^2q}{dt^2} + \epsilon\omega_s(q^2 - 1)\frac{dq}{dt} + \omega_s^2 q - \kappa\frac{\omega_s^4 D\frac{d^2X}{dt^2}}{\omega_s^4 D^2 + \left(\frac{d^2X}{dt^2}\right)^2}q = \frac{A}{D}\frac{d^2Y}{dt^2}. \tag{29}$$

The stability map of Eq.(28), after removing the damping term, with external in-line forcing is plotted in Fig.8(b), with $\kappa = 5$. The stability map is obtained numerically by applying the Floquet theory (Bittanti and Colaneri, 2009). As can be seen in Fig.8(b), the unstable region around $\Omega = 2$ is now bounded. To further illustrate the differences between the two terms, the response of $q$ according to Eqs.(24) and (28) subjected to external forcing at $x_0 = 0.1$ is calculated with $\kappa = 5$ and $\epsilon = 0.08$, and the results are illustrated in Fig.9, where the maximum amplitude of the wake variable $q_{max}$ and the frequency ratio $\Omega_q/\Omega$ ($\Omega_q$ is obtained at the peak frequency) are presented. The results are shown against reduced velocity $V_r$. It is clear that the original in-line coupling term, as depicted in Fig.9(a), results in a lock-in range extended to small reduced velocities, which correspond to high frequency of oscillation, without any sign of lockout. The amplitude of $q$ continuously increases as the reduced velocity decreases, and it reaches a value as high as 11 at $V_r = 0.5$. For the modified coupling term, Fig.9(b) demonstrates that the lock-in range is bounded approximately over the range of reduced velocities between $V_r = 1.5$ and 3.5. The amplification of $q$ only occurs within the lock-in range; outside of this range, $q$ oscillates at an amplitude close to 2.

## 5. Predictions of free vibration experiments using modified in-line coupling

A modified in-line coupling term has been proposed in previous section to solve the stability issue of the original one under forced in-line vibrations. In this section, this modified model

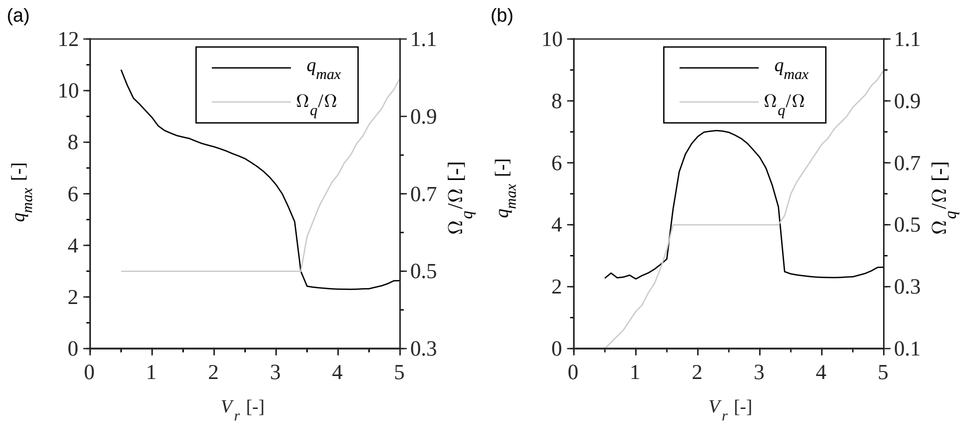


Figure 9: Dynamics of the wake variable $q$ subjected to external in-line forcing at $x_0 = 0.1$ for (a) original in-line coupling term and (b) modified in-line coupling term.

is used to predict free vibration experiments. The simulation cases presented in Section 3 have been repeated with the modified in-line coupling term using the same empirical and tuning parameters. The results are presented in Figs.10-14 in comparison with both experimental results and predictions by the original model.

The modified in-line coupling term has qualitatively similar dynamic characteristics as the original term, therefore it also captures the lock-in regime associated with the in-line vibration mode and the development of super upper branch, as can be seen in Figs.10 and 11. In Fig.10, the predictions of case $m^* = 7$ by the two models are almost exact except that the modified model predicts slightly higher AS in-line amplitudes around $V_n = 2.5$. For the case $m^* = 2.6$, as shown in Fig.11, the model with modified in-line coupling predicts slightly smaller peak amplitudes in both cross-flow and in-line directions. The phase difference between the cross-flow and in-line vibrations predicted by the two models are also almost exact, see Fig.12.

The Griffin plots and variations of the peak amplitude against mass ratios for both cross-flow and in-line vibrations are presented in Figs.13 and 14, where significant differences between predictions by the modified model and those by the original one are observed at small mass ratios. As can be seen in Fig.13, the predicted curves of mass ratios $m^* > 4.5$ are the same for the two models, while the original model predicts significantly larger peak amplitudes at mass ratios $m^* = 3$ and 1.5 in both cross-flow and in-line directions. The influence of the modified in-line coupling term is better presented in Fig.14, where the peak amplitudes that predicted by the original model continuously increase with decreasing mass ratio while those predicted by the modified model reach limits around $1.5D$ and $0.3D$ in cross-flow and in-line directions respectively. It is interesting to notice that the cross-flow peak amplitudes predicted by the modified model start to decrease after reaching a maximum around $1.5D$ at $m^* \approx 2$. Due to the limited data, it is not clear yet whether the same phenomenon was observed in the experiments.

It is not clear yet which model predicts a correct variation trend of the peak amplitude for mass ratios $m^* < 2.5$. However, the experimental data around $m^* = 3$, as previously mentioned in Section 3.2, seem to indicate that the peak amplitude has a tendency of convergence as the mass ratio is further reduced, which is more consistent with the predictions of the modified model. It must be clarified that the modification of the in-line coupling term to formulate a bounded unstable region is purely a mathematical manipulation, and whether the underlying mechanism of VIV in reality is in the same form is not known. However, the modified in-line coupling term does solve the limitation of the original one under forced in-line vibrations at high frequencies and also improves the performance of the model in the predictions of free vibrations at small mass ratios.

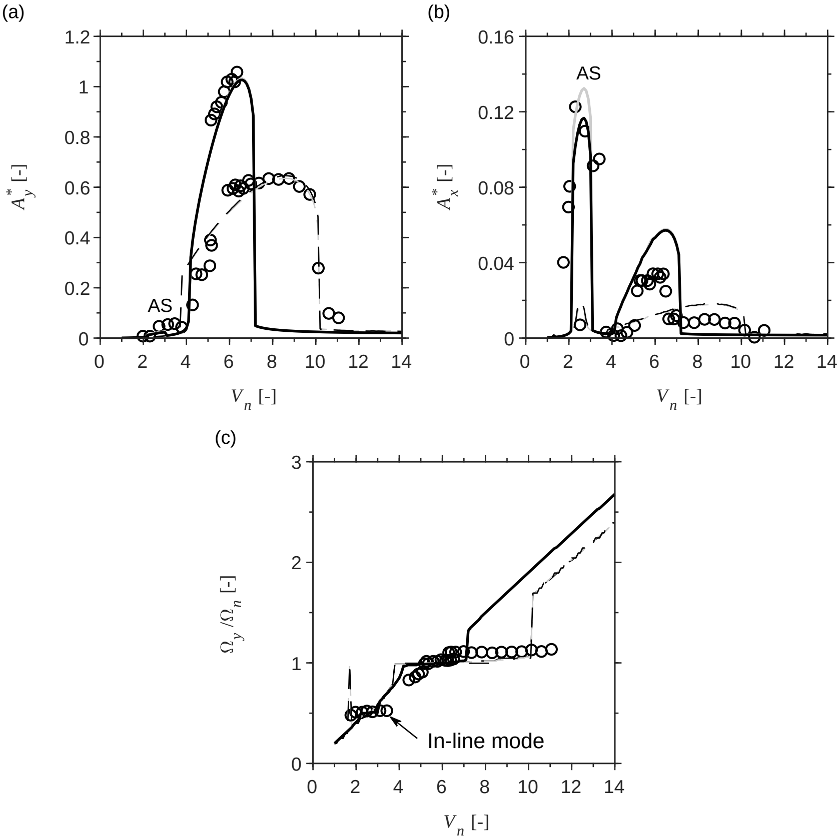


Figure 10: A comparison of numerical (lines) and experimental responses (circles) with $m^* = 7$ and $(m^* + C_a)\zeta = 0.0117$ for (a) Cross-flow response amplitude, (b) In-line response amplitude and (c) Normalized cross-flow response frequency. Solid lines represent "Case U", dashed lines represent "Case L", circles represent experimental data. Black lines represent results from modified model and grey lines represent results from original model.

## 6. Conclusions

In this paper, a new wake oscillator model for the prediction of coupled cross-flow and in-line vortex-induced vibrations (VIV) of an elastically supported rigid cylinder has been proposed and

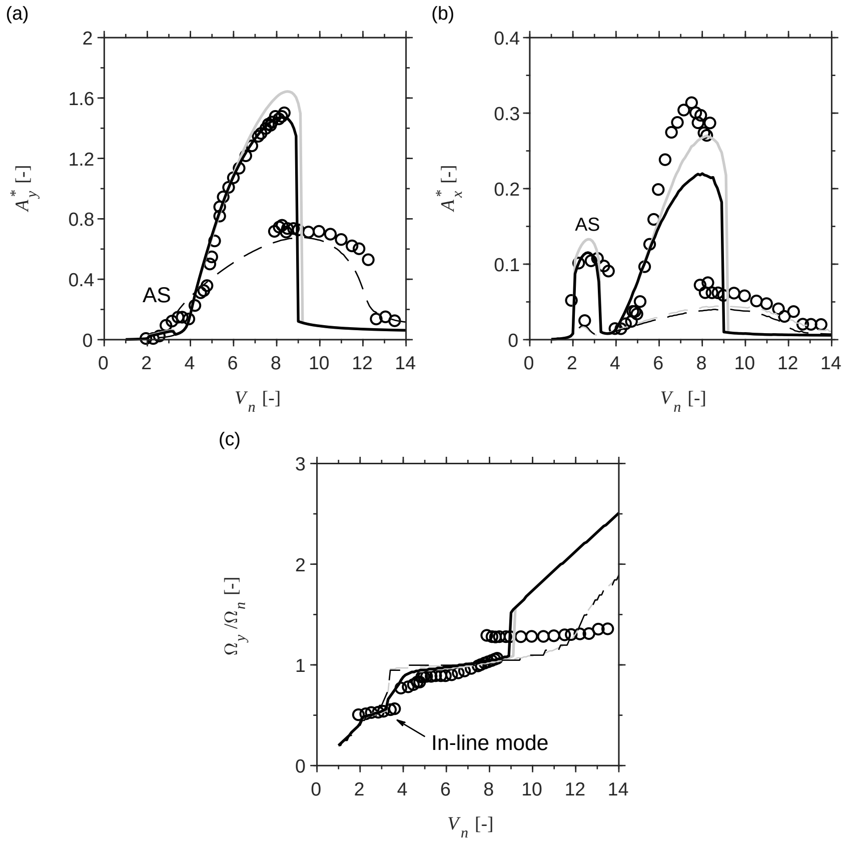


Figure 11: A comparison of numerical (lines) and experimental responses (circles) with $m^* = 2.6$ and $(m^* + C_a)\zeta = 0.013$ for (a) Cross-flow response amplitude, (b) In-line response amplitude and (c) Normalized cross-flow response frequency. Solid lines represent "Case U", dashed lines represent "Case L", circles represent experimental data. Black lines represent results from modified model and grey lines represent results from original model.

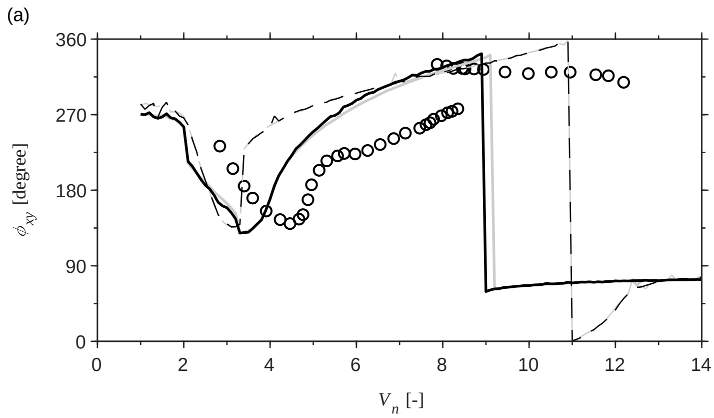


Figure 12: Phase and trajectory of cross-flow and in-line motions with $m^* = 2.6$ and $(m^* + C_a)\zeta = 0.013$ for (a) phase angle (solid lines represent Case U, dashed lines represent Case L, circles represent experimental data). Black lines represent results from modified model and grey lines represent results from original model.

investigated. The novelty of the model lies in the improvements with respect to the conventional van der Pol wake oscillator that have been achieved by introducing a new in-line coupling term as well as by enhancing the expression for the in-line force such that it can fluctuate when the cylinder moves in the in-line direction only.

Based on the experimental observation and heuristic inference from the dynamics of a pendulum, a nonlinear coupling between the wake variable and the acceleration of the in-line motion of the cylinder has been introduced.

The new model has been tuned to the free vibration experiment of an elastically supported rigid cylinder. Two different sets of tuning parameters have been applied to reproduce the upper and lower branches separately. It has been shown that the simulation results are in good agreement with the experimental measurements, and the main characteristics of the coupled cross-flow and in-line VIV are well captured. The simulation results indicate that, in addition to the conventional lock-in range, the proposed model predicts the experimental observation of another lock-in that occurs around reduced velocity of 2.5 due to the in-line vibration. With the same tuning parameters, the model has then been applied to predict another free vibration experiment with smaller mass ratio. It has been demonstrated that the prediction is in good agreement with the experimental measurements. Most importantly, the appearance of the super-upper branch, as a result of the decreasing mass ratio, has been well captured.

The new model has also been compared with experiments regarding the influence of mass and damping ratios on the peak amplitude. The comparison between the Griffin plots generated by the new model and the available experimental data suggests good agreement at moderate and large mass ratios. At very small mass ratios, the model predicts significantly higher peak amplitudes in both cross-flow and in-line directions. The experimental observation of an increasing trend of the peak amplitude as the mass ratio decreases is captured by the proposed model. However, the model predicts continuous increase of cross-flow and in-line peak amplitudes with decreasing mass ratio for $m^* < 2.5$, where the experimental data suggest that the peak amplitude may converge.

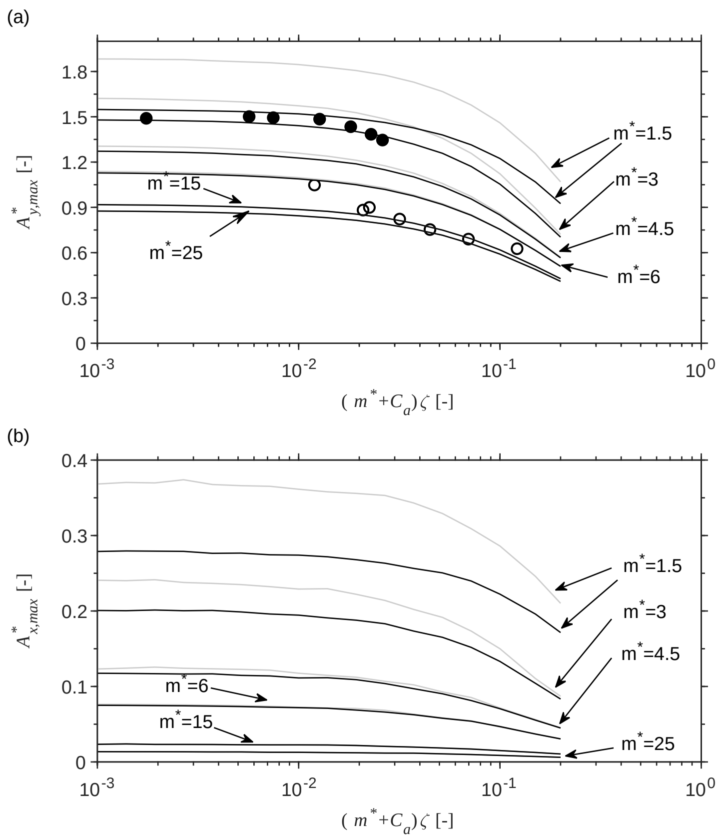


Figure 13: Griffin plots of peak amplitudes for coupled cross-flow and in-line VIV based on experimental (symbols) and prediction (lines) results for (a) Cross-flow peak amplitude and (b) In-line peak amplitude. Dots represent experimental data for $2.5 < m^* < 4$, and circles represent experimental data for $6 < m^* < 25$. Black lines represent results from modified model and grey lines represent results from original model.

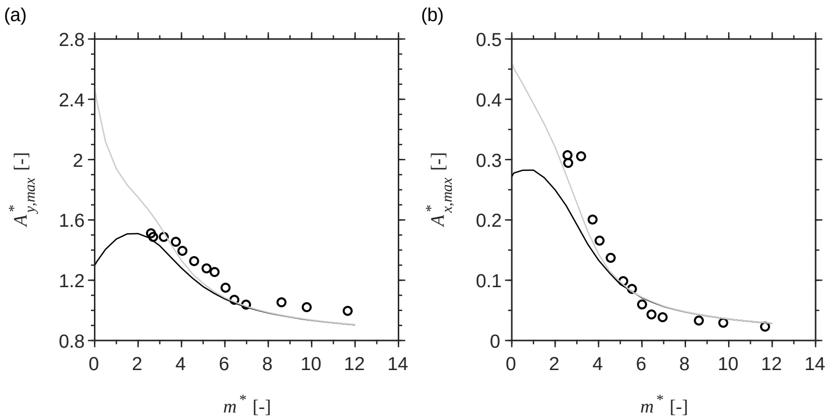


Figure 14: A comparison of predicted (lines) and experimentally measured (dots) peak amplitudes with varying mass ratio for (a) Cross-flow peak amplitude and (b) In-line peak amplitude. Black lines represent results from modified model and grey lines represent results from original model.

Despite of its good performance in the modelling of free vibration of an elastically supported rigid cylinder, the new model has been shown not to be in agreement with experimental observations when subjected to forced in-line vibrations at high frequencies. A modified in-line coupling has been proposed as a remedy for this limitation. The modified in-line coupling has qualitatively similar dynamic characteristics as the original model and is shown to be able to reproduce the free vibration experiments well. Most importantly, at very small mass ratios, the modified in-line coupling predicts a non-increasing trend of the peak amplitude, which is more consistent with experimental observations compared to the original model. Therefore, the modified model is recommended for the modelling of coupled cross-flow and in-line VIV.

To conclude, one can say that the new wake oscillator model presented in this paper shows advantages over the existing wake oscillator models at some aspects. The main superior aspects of the proposed model are its ability to predict the super-upper branch without changing tuning parameters, its ability to predict the lock-in around reduced velocity 2.5 and its physical consistency with the fact that the hydrodynamic forcing in both in-line and cross-flow directions is a result of one and the same fluid motion, which is described in the model by a single oscillator equation. As a preliminary study, the results presented in this paper is not extensive. A more in-depth analysis of the new model, such as comprehensive parametric sensitivity analysis and calibration with more experiments are recommended for future research.

## 7. Acknowledgements

The first author would like to thank the China Scholarship Council (CSC) (No. 201206450001) and Delft University of Technology for the financial support to this work.

## Appendix A. Similarity between the wake oscillator and a rigid pendulum

Consider a rigid pendulum with mass $m_f$ that is attached to a foundation with mass $m_s$ that is elastically supported in X and Y directions; see Fig.A.15. The governing equations for the small vibrations of the system can be derived using the Lagrangian formalism, and they are given as

$$\left(m_s + m_f\right)\frac{d^2X}{dt^2} + k_sX = m_fL\left(\phi\frac{d^2\phi}{dt^2} + \left(\frac{d\phi}{dt}\right)^2\right), \tag{A.1}$$

$$\left(m_s + m_f\right)\frac{d^2Y}{dt^2} + k_sY = -m_fL\frac{d^2\phi}{dt^2}, \tag{A.2}$$

$$m_fL^2\frac{d^2\phi}{dt^2} + m_fgL\phi - m_fL\frac{d^2X}{dt^2}\phi = -m_fL\frac{d^2Y}{dt^2}. \tag{A.3}$$

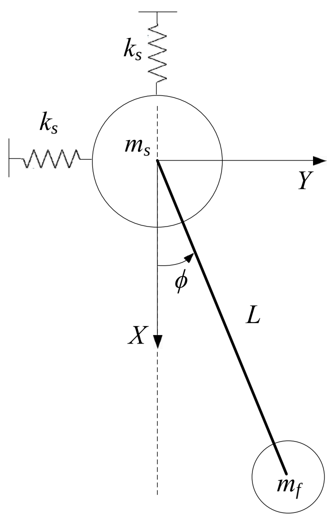


Figure A.15: Pendulum with moving foundation

Using the following relationship:

$$\tau = t\omega_n; \quad \Omega = \frac{\omega_\phi}{\omega_n}; \quad x = \frac{X}{D}; \quad y = \frac{Y}{D}; \tag{A.4}$$

where $\omega_n = \sqrt{k_s/\left(m_s + m_f\right)}$ and $\omega_\phi = \sqrt{m_fg/\left(m_fL\right)}$, the dimensionless form of the equations of the motion is obtained as

$$\ddot{x} + x = M\left(\ddot{\phi}\phi + \dot{\phi}^2\right), \tag{A.5}$$

$$\ddot{y} + y = -M\ddot{\phi}, \tag{A.6}$$

$$\ddot{\phi} + \Omega^2\phi - \ddot{x}\phi = -\ddot{y}, \tag{A.7}$$

where $M = \frac{m_f L}{(m_s+m_f)D}$.

If only the motion of the foundation in the Y direction is considered, corresponding to the VIV that is constrained to the cross-flow direction, then the equations of motion become

$$\ddot{y} + y = -M\ddot{\phi}, \tag{A.8}$$

$$\ddot{\phi} + \Omega^2\phi = -\ddot{y}. \tag{A.9}$$

The above two equations are symmetrically coupled through acceleration; therefore, they are stable. However, if the sign of the pendulum mass is artificially changed from positive to negative, i.e. from $m_f$ to $-m_f$, then Eqs.(A.8) and (A.8) become

$$\ddot{y} + y = M\ddot{\phi}, \tag{A.10}$$

$$\ddot{\phi} + \Omega^2\phi = -\ddot{y}. \tag{A.11}$$

If the above equations are compared to the following simplified form of the wake oscillator equation given by de Langre (2006)

$$\ddot{y} + y = \hat{M}\Omega^2 q, \tag{A.12}$$

$$\ddot{q} + \Omega^2 q = A\ddot{y}, \tag{A.13}$$

then the similarity between the two is obvious. Both systems predict a coupled mode flutter, which, according to de Langre (2006), is the possible fundamental mechanism of VIV.

The similarity between the wake oscillator model and a rigid pendulum with a negative mass for the cross-flow vibration, as described above, provides a possible way in which to derive the form of coupling between the wake oscillator equation and the in-line motion. By changing $m_f$ to $-m_f$, the equations of the motion of the system in the X direction are given as

$$\ddot{x} + x = -M\left(\ddot{\phi}\phi + \dot{\phi}^2\right), \tag{A.14}$$

$$\ddot{\phi} + \Omega^2\phi - \ddot{x}\phi = 0, \tag{A.15}$$

From the above equations, it can be seen that the coupling between the oscillator equation and the in-line motion can be most likely expressed in the form $-\ddot{x}q$, and the force in the in-line direction is in the form $-\left(\ddot{q}q + \dot{q}^2\right)$. For the sake of simplification, as well as for easy implementation, the form of in-line force used in this paper is $q^2$, which has the same phase as $-\ddot{q}q$, while the term $\dot{q}^2$ is neglected. Further research is needed to determine whether using $-\left(\ddot{q}q + \dot{q}^2\right)$ instead of $q^2$ will improve the results. For the cross-flow vibration, the same form as that given by Eqs.(A.12) and (A.13) is still followed. Additional studies are also required to find out whether Eqs.(A.10) and (A.11) are more appropriate for the modelling of cross-flow VIV.

## References

Aguirre Romano, J. E. (1978). *Flow-induced, in-line vibrations of a circular cylinder*. PhD thesis, Imperial College London.

Aronsen, K. H. (2007). *An Experimental Investigation of In-line and Combined In-line and Cross-flow Vortex Induced Vibrations*. PhD thesis, Norwegian University of Science and Technology.

Bai, X. and Qin, W. (2014). Using vortex strength wake oscillator in modelling of vortex induced vibrations in two degrees of freedom. *European Journal of Mechanics - B/Fluids*, 48(Supplement C):165–173.

Birkhoff, G. (1953). Formation of vortex streets. *Journal of Applied Physics*, 24(1):98–103.

Bishop, R. E. D. and Hassan, A. Y. (1964). The lift and drag forces on a circular cylinder oscillating in a flowing fluid. *Proceedings of the Royal Society of London A: Mathematical, Physical and Engineering Sciences*, 277(1368):51–75.

Bittanti, S. and Colaneri, P. (2009). Floquet theory and stability. In *Periodic Systems: Filtering and Control*, pages 81–108. Springer London, London.

Dahl, J., Hover, F., and Triantafyllou, M. (2006). Two-degree-of-freedom vortex-induced vibrations using a force assisted apparatus. *Journal of Fluids and Structures*, 22(6):807–818. Bluff Body Wakes and Vortex-Induced Vibrations (BBVIV-4).

Dahl, J. M., Hover, F. S., Triantafyllou, M. S., Dong, S., and Karniadakis, G. E. (2007). Resonant vibrations of bluff bodies cause multivortex shedding and high frequency forces. *Physical review letters*, 99(14):144503.

de Langre, E. (2006). Frequency lock-in is caused by coupled-mode flutter. *Journal of Fluids and Structures*, 22(6):783–791. Bluff Body Wakes and Vortex-Induced Vibrations (BBVIV-4).

Facchinetti, M., de Langre, E., and Biolley, F. (2004). Coupling of structure and wake oscillators in vortex-induced vibrations. *Journal of Fluids and Structures*, 19(2):123–140.

Gabbai, R. and Benaroya, H. (2005). An overview of modeling and experiments of vortex-induced vibration of circular cylinders. *Journal of Sound and Vibration*, 282(3):575–616.

Govardhan, R. N. and Williamson, C. H. K. (2006). Defining the modified Griffin plot in vortex-induced vibration: revealing the effect of Reynolds number using controlled damping. *Journal of Fluid Mechanics*, 561:147–180.

Hartlen, R. and Currie, I. (1970). Lift-oscillator of vortex-induced vibration. *Journal of the Engineering Mechanics Division*, 96(5):577–591.

Iwan, W. and Blevins, R. (1974). A Model for Vortex Induced Oscillation of Structures. *Journal of Applied Mechanics*, 41(3):581–586.

Jauvtis, N. and Williamson, C. H. K. (2004). The effect of two degrees of freedom on vortex-induced vibration at low mass and damping. *Journal of Fluid Mechanics*, 509:23–62.

Kim, W.-J. and Perkins, N. (2002). Two-dimensional vortex-induced vibration of cable suspensions. *Journal of Fluids and Structures*, 16(2):229–245.

Konstantinidis, E. (2014). On the response and wake modes of a cylinder undergoing streamwise vortex-induced vibration. *Journal of Fluids and Structures*, 45:256–262.

Kovacic, I., Rand, R., and Mohamed Sah, S. (2018). Mathieu's equation and its generalizations: Overview of stability charts and their features. *Applied Mechanics Reviews*, 70(2):020802.

Kurushina, V., Pavlovskaia, E., Postnikov, A., and Wiercigroch, M. (2018). Calibration and comparison of viv wake oscillator models for low mass ratio structures. *International Journal of Mechanical Sciences*, 142-143:547 – 560.

Landl, R. (1975). A mathematical model for vortex-excited vibrations of bluff bodies. *Journal of Sound and Vibration*, 42(2):219–234.

Nishi, Y., Kokubun, K., Hoshino, K., and Uto, S. (2008). Quasisteady theory for the hydrodynamic forces on a circular cylinder undergoing vortex-induced vibration. *Journal of Marine Science and Technology*, 14(3):285–295.

Nishihara, T., Kaneko, S., and Watanabe, T. (2005). Characteristics of fluid dynamic forces acting on a circular cylinder oscillated in the streamwise direction and its wake patterns. *Journal of Fluids and Structures*, 20(4):505–518. Bluff-Body/Flow Interactions.

Ogink, R. and Metrikine, A. (2010). A wake oscillator with frequency dependent coupling for the modeling of vortex-induced vibration. *Journal of Sound and Vibration*, 329(26):5452–5473.

Postnikov, A., Pavlovskaia, E., and Wiercigroch, M. (2017). 2DOF CFD calibrated wake oscillator model to investigate vortex-induced vibrations. *International Journal of Mechanical Sciences*, 127(Supplement C):176–190. Special Issue from International Conference on Engineering Vibration - ICoEV 2015.

Qin, L. (2004). *Development of Reduced-Order Models for Lift and Drag on Oscillating Cylinders with Higher-Order Spectral Moments*. PhD thesis, Virginia Polytechnic Institute and State University.

Sarpkaya, T. (2004). A critical review of the intrinsic nature of vortex-induced vibrations. *Journal of Fluids and Structures*, 19(4):389–447.

Skop, R. and Balasubramanian, S. (1997). A new twist on an old model for vortex-excited vibrations. *Journal of Fluids and Structures*, 11(4):395–412.

Skop, R. and Griffin, O. (1973). A model for the vortex-excited resonant response of bluff cylinders. *Journal of Sound and Vibration*, 27(2):225–233.

Srinil, N. and Zanganeh, H. (2012). Modelling of coupled cross-flow/in-line vortex-induced vibrations using double duffing and van der pol oscillators. *Ocean Engineering*, 53(Supplement C):83–97.

Triantafyllou, M. S., Grosenbaugh, M. A., and Gopalkrishnan, R. (1994). Vortex-induced vibrations in a sheared flow: a new predictive method. In *Hydroelasticity in Marine Technology*.

Williamson, C. and Govardhan, R. (2004). Vortex-induced vibrations. *Annual Review of Fluid Mechanics*, 36(1):413–455.

Wu, Z. and Moe, G. (1990). The lift force on a cylinder vibrating in a current. *Journal of Offshore Mechanics and Arctic*

*Engineering*, 112(4):297–303.